

# Micro mechanics of isotropic normal compression

G. R. MCDOWELL\*, J. P. DE BONO\*, P. YUE\* and H-S. YU\*

Discrete element modelling has been used to investigate the micro mechanics of isotropic normal compression. One-dimensional (1D) normal compression has previously been modelled in three dimensions using an oedometer and a large number of particles and without the use of agglomerates, and it was shown that the compression index was solely related to the strengths of the particles as a function of size. The same procedure is used here to model isotropic normal compression. The fracture of a particle is governed by the octahedral shear stress within the particle (due to the multiple contacts) and a Weibull distribution of strengths. The octahedral shear stresses, due to local anisotropic stresses within a sample with isotropic boundary stresses, are shown to give rise to a normal compression line (NCL) and the evolution of a distribution of particle sizes. The compression line is parallel to the 1D NCL in  $\log e$ - $\log p$  space, in agreement with traditional critical state soil mechanics and confirming that the compression index is solely a function of the size effect on average particle strength, which determines the hardening law for the material. The paper shows, for the first time, how local octahedral shear stresses induced in the particles within the sample generate an isotropic normal (clastic) compression line.

**KEYWORDS:** compressibility; discrete-element modelling; fractals; numerical modelling; particle crushing/crushability; particle-scale behaviour

ICE Publishing: all rights reserved

## NOTATION

$b$	size effect on strength for a material
$D$	fractal dimension
$d$	particle size (diameter)
$d_0$	initial particle size
$e$	voids ratio
$e_y$	voids ratio corresponding to the yield stress on the linear $\log e$ - $\log \sigma$ plot
$F$	force
$F_j^{(c)}$	force at a contact
$L$	particle size
$m$	Weibull modulus
$N$	number of particles
$N_c$	number of contacts on a particle
$p$	mean stress
$q$	octahedral shear stress in a particle
$q_m$	mean octahedral shear stress
$q_0$	value of octahedral shear stress such that 37% of particles are stronger for a given particle size
$V$	volume of a particle
$x_i^{(c)}$	location of the contact
$x_i^{(p)}$	location of the particle
$\sigma$	stress
$\sigma_f$	tensile stress at failure
$\sigma_{ij}$	stress tensor for a particle
$\sigma_m$	mean strength
$\sigma_0$	value of tensile stress such that 37% of particles are stronger for a given particle size
$\sigma_1$	major principal stress in a particle
$\sigma_2$	intermediate principal stress in a particle
$\sigma_3$	minor principal stress in a particle
$\sigma_y$	yield stress on the $\log e$ - $\log \sigma$ plot

## INTRODUCTION

Crushing has generally been modelled using the discrete element method (DEM) via the two alternative methods of

- replacing ‘breaking’ grains with new, smaller fragments, generally in two-dimensions (Åström & Herrmann, 1998; Tsoungui *et al.*, 1999; Lobo-Guerrero & Vallejo, 2005; Ben-Nun & Einav, 2010; Ben-Nun *et al.*, 2010)
- using three-dimensional (3D) agglomerates (McDowell & Harireche, 2002; Cheng *et al.*, 2003; Bolton *et al.*, 2008).

In the latter method, no consideration was given to the complex distribution of loads on each particle at its multiple contacts. This issue has recently been addressed by McDowell & de Bono (2013) who allowed particles to fracture without the use of agglomerates and by considering the stresses induced in a particle due to the multiple contacts. McDowell & de Bono (2013) allowed each particle to split into new fragments, without loss of mass when the value of the induced particle stress was found to be greater than or equal to its strength. The new sphere fragments overlap enough to be contained within the bounding parent sphere (in the case of two fragments, for example, the axis joining the centres of the new spheres is aligned along the direction of the minor principal stress). This produces local pressure spikes during breakage; however, the overlap causes the fragments to move along the direction of the minor principal stress for the original particle, just as would occur for a single particle crushed between platens, and the excess energy is transferred to the surrounding particles. Although conservation of energy is not observed in this case, the goal was to achieve an effective breakage mechanism that was as simple and realistic as possible. As several authors (e.g. Åström & Herrmann, 1998) have conjectured, it is not possible to simulate perfectly realistic fracture using self-similar fragments. To ensure sample stability, McDowell & de Bono (2013) updated particle breakages at once (for the whole sample) after a minimum required number of computational

Manuscript received 2 July 2013; first decision 16 August 2013; accepted 2 October 2013.

Published online at [www.geotechniqueletters.com](http://www.geotechniqueletters.com) on 29 October 2013.

\*University of Nottingham, Nottingham, UK

timesteps to allow the artificially induced energy to dissipate; full details can be found in McDowell & de Bono (2013).

The compression of sand is associated with the evolution of a particle size distribution; this has been linked in the past to work equations that account for the dissipation of energy via friction, the creation of surface resulting from breakage (e.g. McDowell & Bolton, 1998) and the redistribution of loads (e.g. Russell, 2011; Ovalle *et al.*, 2013). Crushing during shearing has long been associated with the evolution of *fractal* particle size distributions (e.g. Turcotte, 1986; McDowell & Daniell, 2001), and both McDowell & Bolton (1998) and Russell (2011) linked the linear slope (in  $e$ -log  $\sigma$  space) of the normal compression line (NCL) to the theory of fractal crushing using their respective energy equations.

McDowell (2005) used the kinematics of particle fracture and the associated void collapse along with fractal crushing theory to show, analytically, that the one-dimensional (1D) NCL should actually be linear in log  $e$ -log  $\sigma$  space, which was validated by McDowell & de Bono (2013) who used the DEM to link the compression of sand to the evolution of a fractal distribution of particles. The influence of the mechanics of fracture on the slope of the NCL was thoroughly investigated, and is briefly described here, and the model therein applied to the isotropic compression of aggregates.

#### PARTICLE STRENGTHS

McDowell & Amon (2000) demonstrated that Weibull (1951) statistics can successfully be applied to the fracture of soil grains. It is widely accepted that the failure of a spherical particle under pure compression is tensile, and that fractures initiate from existing flaws and the associated stress concentrations. Assuming that failure of particles occurs by fast fracture under induced tensile stresses, McDowell & Amon (2000) obtained the survival probability for a particle under diametral compression by integration of the probability function as a function of induced tensile stress over the volume of the particle under tension; they showed that the Weibull size effect is still valid for such loading, assuming that particles are similar in shape and are loaded in the same way. Jaeger (1967) proposed that the tensile strength of grains could be measured by diametral compression between flat platens as

$$\sigma_f = \frac{F}{d^2} \quad (1)$$

where  $\sigma_f$  is the tensile stress at failure,  $F$  is the diametral compressive force applied by the platens and  $d$  is the diameter of the grain at failure. Using this equation, McDowell & Bolton (1998) reported that the tensile strengths obtained from single particles of various sizes crushed between flat platens could be related to size by

$$\sigma_m \propto d^b \quad (2)$$

where  $\sigma_m$  is the mean strength and  $b$  describes the size-hardening law (after Billam, 1972; Lee, 1992). Weibull distributions are described by two parameters – one defining the shape of the distribution, usually termed the Weibull modulus  $m$ , which is related directly to the coefficient of variation, and the other defining the scale, which is a characteristic value of the distribution such that 37% (i.e.  $\exp(-1)$ ) of random variables are greater (in the case of particle strengths this determines the 37% survival probability), and is proportional to the mean. For a given 37% strength, increasing the Weibull modulus decreases the

variability in strengths. From Weibull's survival probability for a block of material under tension, it is possible to derive the following relation

$$\sigma_0 \propto d^{-3/m} \quad (3)$$

where  $\sigma_0$  is the value of tensile stress at which 37% of the total number of particles of size  $d$  survive and  $m$  is the Weibull modulus (assuming bulk fracture dominates and Weibull therefore gives a volume 'effect' on particle strength (McDowell & Bolton, 1998)). McDowell & Amon (2000) and McDowell (2002) confirmed that equation (3) could be applied to sand particles by single particle crushing tests.

In the two-dimensional models mentioned earlier, various fracture criteria were used; some authors used a measure of shear stress (e.g. Tsoungui *et al.*, 1999; Lobo-Guerrero & Vallejo, 2005) while Åström & Herrmann (1998) and Ben-Nun & Einav (2010) additionally investigated using a measure of the compressive stress on a grain (although both reported that the final particle size distributions from their simulations were largely unaffected by the fracture criterion). Russell *et al.* (2009), on the other hand, presented an analysis of idealised, regular granular assemblies and suggested that the failure criterion for brittle materials is related to the maximum single contact force. In 3D work using agglomerates (e.g. Lim & McDowell, 2004; Bolton *et al.*, 2008), although agglomerates could break under complex distributions of loads, no consideration was given to the stress induced by multiple contacts. McDowell *et al.* (1996) showed that, for fractal crushing, it is the coordination number that is the dominant factor influencing the probability of fracture for a particle (the likelihood of fracture increasing with reducing coordination number). McDowell & de Bono (2013) therefore decided that if a particle is loaded uniformly over its surface and is under a high hydrostatic stress but low deviatoric stress, it would be unlikely to break. They stated that it would therefore not be realistic to use the mean stress to establish whether a particle would break or not (or the maximum principal stress), as this would mean the fracture criterion would be unaffected even if the other principal stresses were of equal magnitude. They decided to use the average octahedral shear stress induced within each sphere to determine whether fracture should occur or not. The octahedral shear stress is derived from the average principal stresses within a particle and is given by

$$q = \frac{1}{3} \left[ (\sigma_1 - \sigma_2)^2 + (\sigma_2 - \sigma_3)^2 + (\sigma_1 - \sigma_3)^2 \right]^{1/2} \quad (4)$$

This means that if a particle is, for example under diametral point loads, equal in three mutually orthogonal directions, then the particle would not break under this hydrostatic stress ( $q = 0$ ). Although the stresses in a spherical particle vary as a function of position within the volume of the particle (e.g. Jaeger, 1967; Russell *et al.*, 2009), the simplification of using the average octahedral shear stress provides a simple criterion to facilitate breakage, taking into account multiple contacts and different contact forces on a particle surface while avoiding the use of agglomerates. In this paper it will be shown that even for isotropic boundary stresses, local anisotropic stresses give rise to crushing, according to equation (4). In PFC3D (Itasca, 2005), the average stress tensor in a particle is

$$\sigma_{ij} = \frac{1}{V} \sum_{N_c} \left| x_i^{(c)} - x_i^{(p)} \right| n_i^{(c,p)} F_j^{(c)} \quad (5)$$

where  $V$  is the volume of the particle,  $N_c$  is the number of contacts,  $x_i^{(c)}$  and  $x_i^{(p)}$  are the locations of the contact and particle respectively,  $n_i^{(c,p)}$  is the unit-normal vector directed from the particle centroid to the contact location and  $F_j^{(c)}$  is the force at the contact (Itasca, 2005). For the case of a particle compressed diametrically between platens, the major principal stress is

$$\sigma_{11} = \frac{1}{(\pi/6)d^3} F \frac{d}{2} = \frac{6F}{\pi d^2} \quad (6)$$

From equation (4), it can be seen that the value of octahedral shear stress  $q$  for a sphere compressed diametrically between two walls is then given by

$$q = \frac{2^{1/2}}{3} \left( \frac{6F}{\pi d^2} \right) = 0.9 \frac{F}{d^2} \quad (7)$$

which is the value of  $q$  returned by PFC3D for a sphere compressed between two walls; hence the average octahedral shear stress in a particle is proportional to equation (1). Therefore, McDowell & de Bono (2013) assumed that for particles loaded under multiple contacts, the particle would break if the octahedral shear stress was greater than or equal to its ‘strength’, where the strengths of the particles satisfy a Weibull distribution of  $q$  values and thus a size effect on 37% strength according to equation (3)

$$q_0 \propto d^{-3/m} \quad (8)$$

#### ONE-DIMENSIONAL NORMAL COMPRESSION

McDowell & de Bono (2013) used a mono-disperse sample of 620 spheres of diameter 2 mm, created in a scaled-down oedometer (diameter 30 mm, height 7 mm). The sample was loaded one-dimensionally. Different strength characteristics, hardening laws and mechanisms of fracture were used to investigate their influence on the particle size distribution resulting from crushing and the slope of the NCL for the simulations. The initial sample was created using the radii expansion technique (Itasca, 2005), resulting in a dense, random packing that was subjected to a number of explicit time-stepping cycles to remove any locked-in forces or overlap. Using a larger sample with more particles appeared to give the same compression behaviour, but simulations were unable to reach high pressures due to the large number of particles covering such a wide range of scales. McDowell & de Bono (2013) investigated the initial characteristic strength of the particles  $q_0$ , the initial grading (hence particle size), the fracture mechanism and the distribution of strengths (assuming that the size effect on average strength was governed separately) – all of which

**Table 1.** DEM parameters for simulations of 1D and isotropic normal compression

Particle diameter, $d_0$ : mm	2
Particle density: $\text{kg/m}^3$	2650
Initial number of particles	620
Voids ratio, $e_0$	0.82
Shear modulus, $G$ : GPa	28
Poisson’s ratio, $\nu$	0.25
Particle friction coefficient	0.5
Wall friction coefficient	0
Weibull modulus, $m$	3.3
37% strength, $q_0$ : MPa	37.5

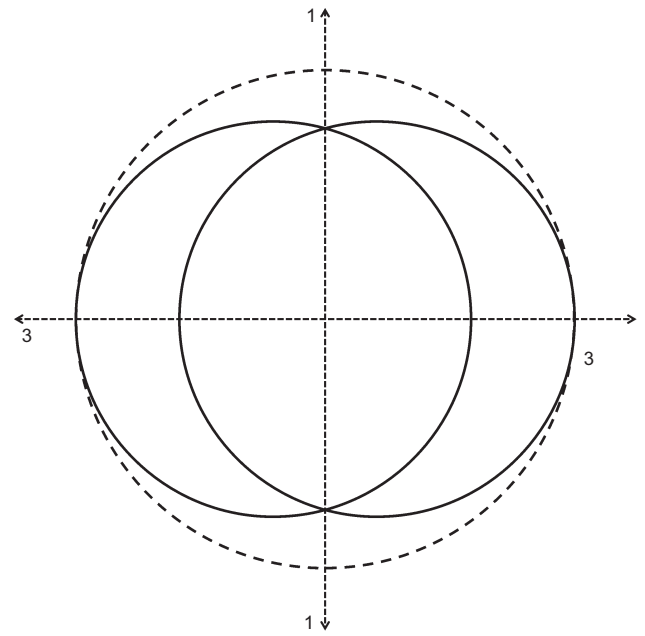


**Fig. 1.** Equal diametral splitting mechanism

had no influence on the compressibility index or the final particle size distributions. Most significantly, McDowell & de Bono (2013) examined a range of hardening laws and showed that if the mean particle strength  $q_m$  is related to size  $d$  by a law of the form

$$q_m \propto d^{-b} \quad (9)$$

then 1D compression can be described by

$$\log e = \log e_y - \frac{1}{2b} \log \frac{\sigma}{\sigma_y} \quad (10)$$

where  $e_y$  is the value on the linear log–log plot at a stress corresponding to the yield stress  $\sigma_y$ , and  $\sigma_y$  is proportional to the average particle strength. They showed that this was consistent with the evolution of a fractal distribution of particle sizes with a fractal dimension of 2.5 and that equation (10) holds irrespective of the distribution of strengths for a given size; for a given value of  $b$  in equation (9), the distribution of strengths simply governs the rate of onset of yield onto the NCL.

McDowell & de Bono (2013) modelled the 1D compression of silica sand studied earlier by McDowell (2002) using the parameters given in Table 1 and the simple splitting mechanism shown in Fig. 1; these are also used here for isotropic normal compression. The resulting 1D compression line is shown in Fig. 2, plotted on  $\log e$ – $\log \sigma$  axes. The slope is given by the size-hardening law and, in this case, from Table 1,  $b = 3/m = 3/3.3$  according to equation (8), so the slope of the NCL is about 0.5, in agreement with the experimental data of McDowell (2002).

#### ISOTROPIC NORMAL COMPRESSION

The current study takes the same sample as in McDowell & de Bono (2013) and the same crushing criteria as in equation (4) to investigate

- whether the localised anisotropic stresses within an isotropically compressed sample would be sufficient to cause crushing and the development of an isotropic NCL

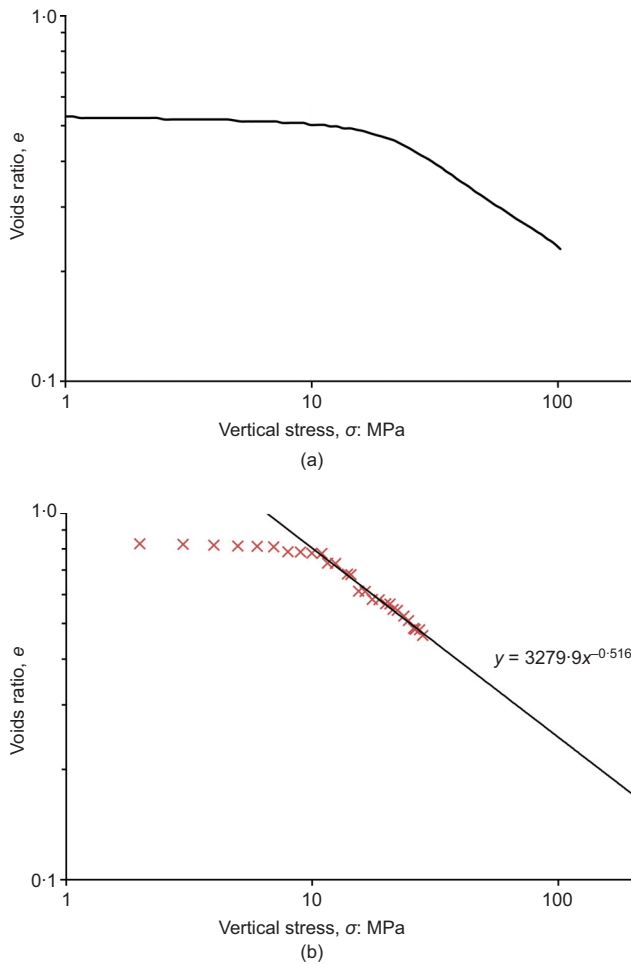


**Fig. 2.** Compression plots for silica sand: (a) from McDowell (2002); (b) from numerical simulation plotted on log  $e$ –log stress axes (McDowell & de Bono, 2013)

- whether such a line might be parallel to the 1D NCL when the logarithm of voids ratio is plotted against the logarithm of mean effective stress
- how high the required boundary stresses might be to cause crushing and normal compression.

The initial sample, identical to that used by McDowell & de Bono (2013), is shown in Fig. 3.

Figure 4 shows the NCL generated for the simulation of the isotropic compression test on silica sand. The NCL for the McDowell & de Bono (2013) 1D simulation is also shown in the same figure (in this case plotted against the logarithm of mean effective stress). It is clear that the isotropic NCL generated using the octahedral shear stress crushing criterion is parallel to the 1D NCL in log  $e$ –log  $p$  space, and both lines have a slope of 0.5. This is reassuring and confirms the proposal made by McDowell & de Bono (2013) that the slope should be a function of the hardening

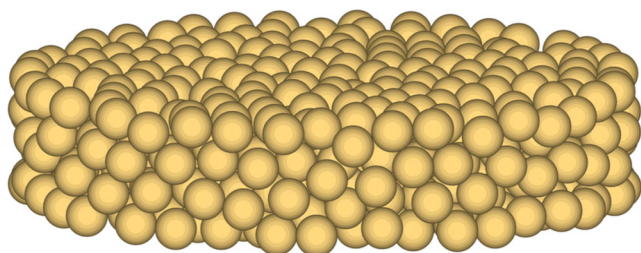


**Fig. 3.** Initial sample before compression

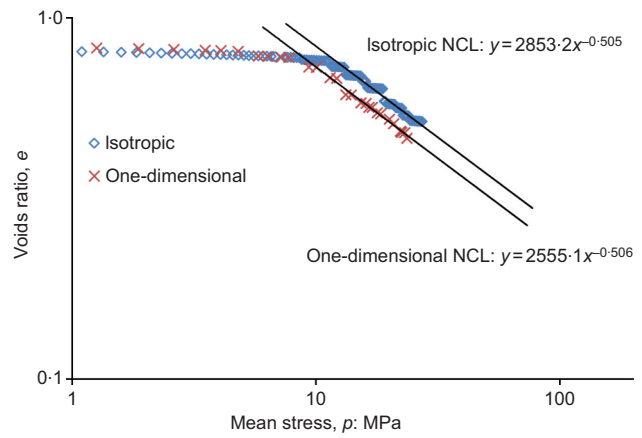


**Fig. 4.** Isotropic normal compression and 1D normal compression plots (on a log–log scale) for simulation on silica sand using the parameters in Table 1

law for the size effect on particle strength, and this should be independent of the loading conditions. The yield stress for the isotropic sample is about 11 MPa, compared with about 8 MPa for the one-dimensionally compressed sample.

The evolution of the particle size distribution was also measured in terms of the percentage of mass of particles smaller than a given size plotted against the logarithm of

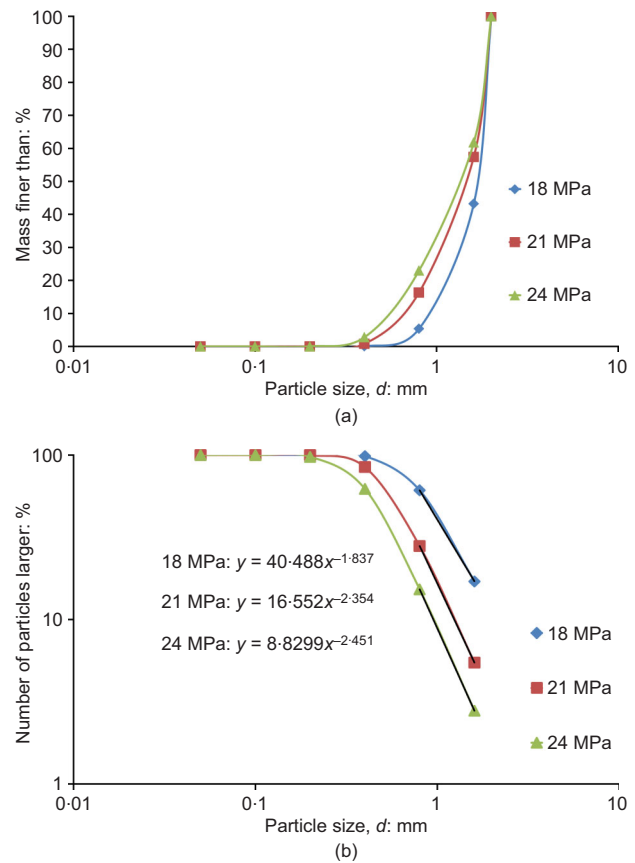


**Fig. 5.** Evolving particle size distributions from isotropic compression: (a) percent by mass of particles finer than size  $d$  plotted against  $d$  on the traditional linear–log scale; (b) percent by number of particles greater than size  $d$  plotted against  $d$  on log–log axes



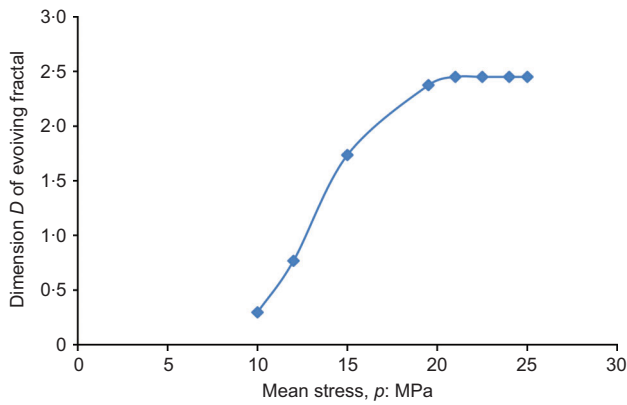


**Fig. 6.** Fractal dimension  $D$  of the evolving particle size distribution (assuming the last two data points in Fig. 5 correspond to a fractal distribution)

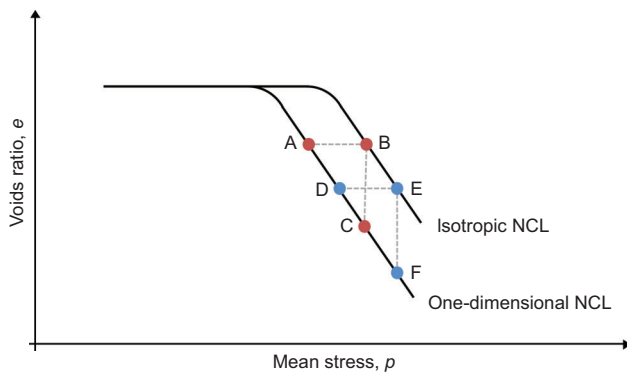


**Fig. 7.** Schematic diagram on log-log axes showing the two sets of data points (A, B, C and D, E, F) at which the particle size distributions are compared

that size, in the traditional way as shown in Fig. 5(a), and also by the percentage of number of particles greater than a given size plotted against size on a log-log scale (Fig. 5(b)). The equations shown in Fig. 5(b) are for the linear parts of the curves (i.e. the last two data points on each plot), and the exponent gives the fractal dimension assuming that the last two data points correspond to a fractal distribution such that

$$N(L > d) \propto d^{-D} \quad (11)$$

where  $N$  is the number of particles of size  $L$  greater than size  $d$ , and  $D$  is the fractal dimension (Turcotte, 1986). A fractal particle size distribution appears to emerge, with an ultimate fractal dimension of 2.5 approached as crushing occurs. This is further illustrated in Fig. 6, which shows

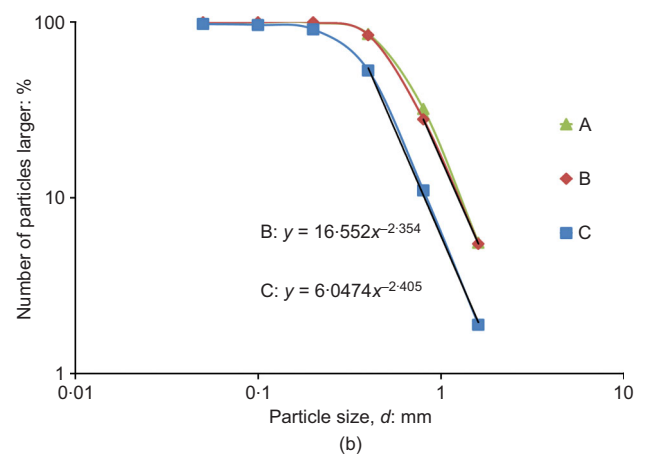
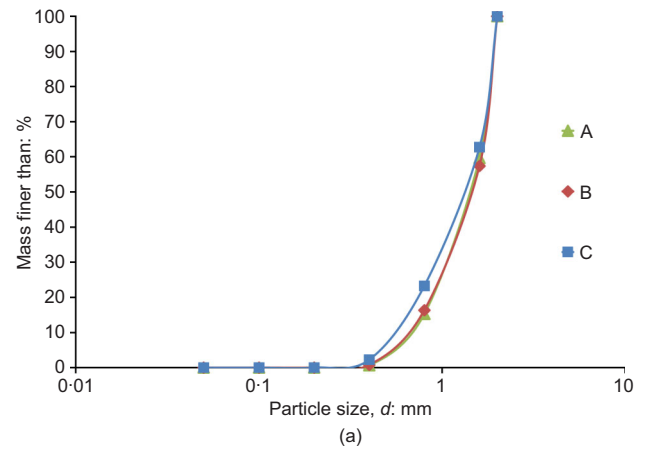


**Fig. 8.** Evolving particle size distributions for points A, B and C: (a) percent by mass of particles finer than size  $d$  plotted against  $d$  on the traditional linear-log scale; (b) percent by number of particles greater than size  $d$  plotted against  $d$  on log-log axes

how the calculated fractal dimension evolves as the stress level is increased; it is consistent with the findings of McDowell & de Bono (2013) for 1D conditions.

To gain further insight into the micro mechanics of isotropic compression and how it relates to the micro mechanics of 1D normal compression, it was decided to take a point (A) on the 1D NCL and a point (B) on the isotropic NCL at the same voids ratio and compare the particle size distributions. A further point (C) on the 1D NCL at the same mean effective stress as point B was also chosen to compare the particle size distribution with that at points A and B. These points are shown schematically in Fig. 7. This procedure was repeated for a further set of points, D, E and F (group 2), and all six data points are summarised in Table 2.

**Table 2.** Data points chosen to compare the particle size distributions

	Group 1			Group 2		
Point	A	B	C	D	E	F
NCL	1D	Isotropic	1D	1D	Isotropic	1D
Voids ratio, $e$	0.565	0.565	0.485	0.525	0.521	0.464
Mean stress, $p$ : MPa	17.0	21.3	21.3	20.0	24.3	24.3

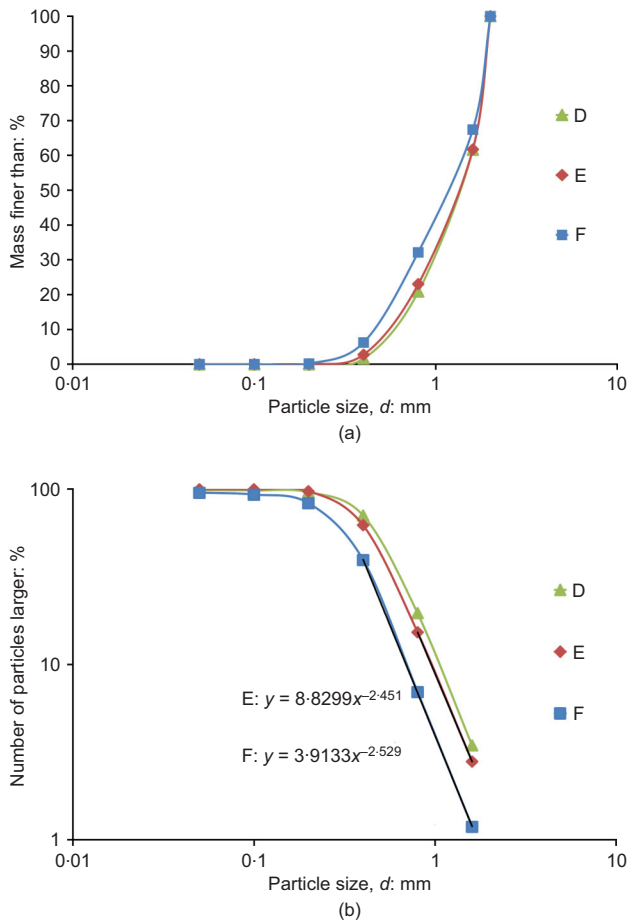


**Fig. 9.** Evolving particle size distributions for points D, E and F: (a) percent by mass of particles finer than size  $d$  against size  $d$  on the traditional linear–log scale; (b) percent by number of particles greater than size  $d$  against size  $d$  on log–log axes

Figure 8 shows the particle size distributions for the first set of data points A, B and C (group 1); the particle size distributions for D, E and F (group 2) are shown in Fig. 9. Both figures illustrate that the points at the same voids ratio on the 1D and isotropic NCLs (i.e. points A and B from group 1 and points D and E from group 2) have particle size distributions that appear to coincide. The distribution of non-zero  $q$  values for all particles is shown for points A and B in Fig. 10(a) and for D and E in Fig. 10(b). Figure 10 demonstrates that when the particle distributions coincide (when the 1D and isotropic simulations reach the same voids ratio), the particles are approximately under the same distribution of local octahedral shear stresses – the distributions of octahedral shear stresses in the particles are similar for pairs A and B and D and E. The figures show that in the new simulations presented in this paper, despite the sample being loaded isotropically, significant local octahedral shear stresses are induced; these are what appear to give rise to crushing and produce the isotropic NCL, parallel to the 1D NCL and with similar particle size distributions at the same voids ratio. Further work will focus on the evolution of the particle size distribution under a wide range of stress paths.

## CONCLUSIONS

Discrete element modelling has been used to investigate the micro mechanics of isotropic normal compression. The

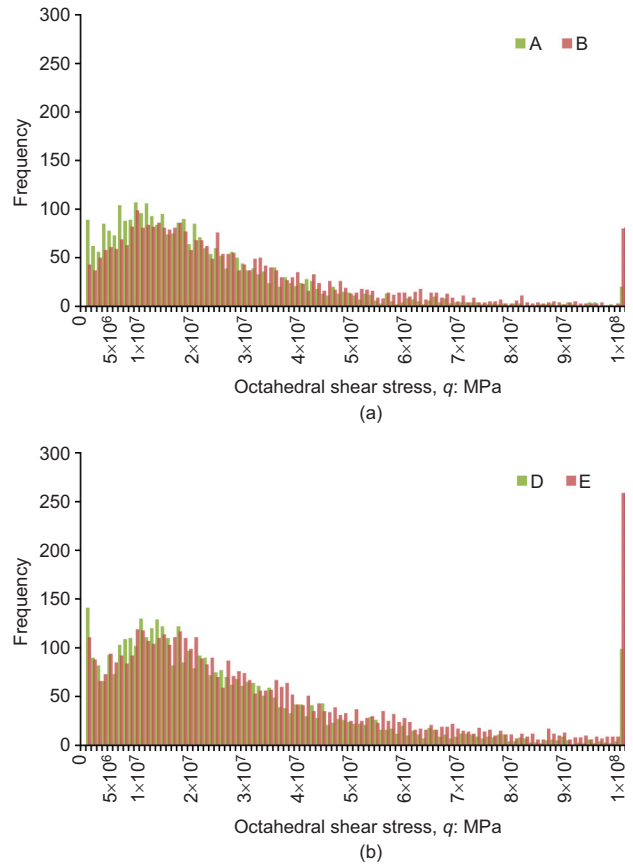


**Fig. 10.** Distribution of octahedral shear stress  $q$  for the particles at points A and B (a) and points D and E (b)

fracture of a particle is governed by the average octahedral shear stress within the particle due to the multiple contacts and a Weibull distribution of strengths. The octahedral shear stresses, due to local anisotropic stresses within a sample with isotropic boundary stresses, have been shown to give rise to an isotropic NCL and the evolution of a distribution of particle sizes. The compression line is parallel to the 1D NCL in  $\log e$ – $\log p$  space, in agreement with traditional critical state soil mechanics and with a slope of 0.5 for the simulated silica sand, as proposed by McDowell (2005) and McDowell & de Bono (2013). This also reinforces the earlier proposition (McDowell & de Bono, 2013) that the compression index should be solely determined by the hardening law for the average particle strength as a function of size, and this should be independent of the loading configurations of the particles for different macroscopic stress ratios. It has therefore been shown – for the first time – how local octahedral shear stresses within an isotropically compressed sample generate an isotropic normal (clastic) compression line.

## REFERENCES

- Åström, J. A. & Herrmann, H. J. (1998). Fragmentation of grains in a two-dimensional packing. *Euro. Phys. J. B* **5**, No. 3, 551–554.
- Ben-Nun, O. & Einav, I. (2010). The role of self-organization during confined comminution of granular materials. *Phil. Trans. R. Soc. A* **368**, No. 1910, 231–247.
- Ben-Nun, O., Einav, I. & Tordesillas, A. (2010). Force attractor in confined comminution of granular materials. *Phys. Rev. Lett.* **104**, No. 10, 108001.
- Billam, J. (1972). Some aspects of the behaviour of granular materials at high pressures. In *Proceedings of the Roscoe*

- Memorial Symposium, Cambridge University* (Parry, R. H. (ed.)). London: G. T. Foulis, pp. 69–80.
- Bolton, M. D., Nakata, Y. & Cheng, Y. P. (2008). Micro- and macro-mechanical behaviour of DEM crushable materials. *Géotechnique* **58**, No. 6, 471–480.
- Cheng, Y. P., Nakata, Y. & Bolton, M. D. (2003). Discrete element simulation of crushable soil. *Géotechnique* **53**, No. 7, 633–641.
- Itasca (2005). *Particle flow code in three dimensions, software manual*. Minnesota, MN: Itasca Consulting Group Inc.
- Jaeger, J. C. (1967). Failure of rocks under tensile conditions. *Int. J. Rock. Mech. Mining Sci.* **4**, No. 2, 219–227.
- Lee, D. M. (1992). *The angles of friction of granular fills*. University of Cambridge.
- Lim, W. L. & McDowell, G. R. (2005). Discrete element modelling of railway ballast. *Granular Matter* **7**, No. 1, 19–29.
- Lobo-Guerrero, S. & Vallejo, L. E. (2005). Crushing a weak granular material: experimental numerical analyses. *Géotechnique* **55**, No. 3, 245–249.
- McDowell, G. R. (2002). On the yielding and plastic compression of sand. *Soils and Found.* **42**, No. 1, 139–145.
- McDowell, G. R. (2005). A physical justification for  $\log e$ – $\log \sigma$  based on fractal crushing and particle kinematics. *Géotechnique* **55**, No. 9, 697–698.
- McDowell, G. R. & Amon, A. (2000). The application of Weibull statistics to the fracture of soil particles. *Soils and Found.* **40**, No. 5, 133–141.
- McDowell, G. & Bolton, M. D. (1998). On the micro mechanics of crushable aggregates. *Géotechnique* **48**, No. 5, 667–679.
- McDowell, G. R. & Daniell, C. M. (2001). Fractal compression of soil. *Géotechnique* **51**, No. 2, 173–176.
- McDowell, G. R. & de Bono, J. P. (2013). On the micro mechanics of one-dimensional normal compression. *Géotechnique* **63**, No. 11, 895–908.
- McDowell, G. & Harireche, O. (2002). Discrete element modelling of soil particle fracture. *Géotechnique* **52**, No. 2, 131–135.
- McDowell, G. R., Bolton, M. D. & Robertson, D. (1996). The fractal crushing of granular materials. *J. Mech. Phys. Solids* **44**, No. 12, 2079–2102.
- Ovalle, C., Dano, C. & Hicher, P.-Y. (2013). Experimental data highlighting the role of surface fracture energy in quasi-static confined comminution. *Int. J. Fracture* **182**, No. 1, 123–130.
- Russell, A. R. (2011). A compression line for soils with evolving particle and pore size distributions due to particle crushing. *Géotechnique Lett.* **1**, No. 1, 5–9.
- Russell, A. R., Muir Wood, D. & Kikumoto, M. (2009). Crushing of particles in idealised granular assemblies. *J. Mech. Phys. Solids* **57**, No. 8, 1293–1313.
- Tsoungui, O., Vallet, D. & Charmet, J.-C. (1999). Numerical model of crushing of grains inside two-dimensional granular materials. *Powder Technol.* **105**, No. 1, 190–198.
- Turcotte, D. L. (1986). Fractals and fragmentation. *J. Geophys. Res.* **91**, No. B2, 1921–1926.
- Weibull, W. (1951). A statistical distribution function of wide applicability. *J. Appl. Mech.* **18**, No. 3, 293–297.

---

#### WHAT DO YOU THINK?

To discuss this paper, please email up to 500 words to the editor at journals@ice.org.uk. Your contribution will be forwarded to the author(s) for a reply and, if considered appropriate by the editorial panel, will be published as a discussion.